LETTER

doi:10.1038/nature20586

The rapid formation of Sputnik Planitia early in Pluto's history

Douglas P. Hamilton[1], S. A. Stern[2], J. M. Moore[3], L. A. Young[2] & the New Horizons Geology, Geophysics & Imaging Theme Team*

Pluto's Sputnik Planitia is a bright, roughly circular feature that resembles a polar ice cap. It is approximately 1,000 kilometres across and is centred on a latitude of 25 degrees north and a longitude of 175 degrees, almost directly opposite the side of Pluto that always faces Charon as a result of tidal locking[1]. One explanation for its location includes the formation of a basin in a giant impact, with subsequent upwelling of a dense interior ocean[2]. Once the basin was established, ice would naturally have accumulated there[3]. Then, provided that the basin was a positive gravity anomaly (with or without the ocean), true polar wander could have moved the feature towards the Pluto–Charon tidal axis, on the far side of Pluto from Charon[2,4]. Here we report modelling that shows that ice quickly accumulates on Pluto near latitudes of 30 degrees north and south, even in the absence of a basin, because, averaged over its orbital period, those are Pluto's coldest regions. Within a million years of Charon's formation, ice deposits on Pluto concentrate into a single cap centred near a latitude of 30 degrees, owing to the runaway albedo effect. This accumulation of ice causes a positive gravity signature that locks, as Pluto's rotation slows, to a longitude directly opposite Charon. Once locked, Charon raises a permanent tidal bulge on Pluto, which greatly enhances the gravity signature of the ice cap. Meanwhile, the weight of the ice in Sputnik Planitia causes the crust under it to slump, creating its own basin (as has happened on Earth in Greenland[5]). Even if the feature is now a modest negative gravity anomaly, it remains locked in place because of the permanent tidal bulge raised by Charon. Any movement of the feature away from 30 degrees latitude is countered by the preferential recondensation of ices near the coldest extremities of the cap. Therefore, our modelling suggests that Sputnik Planitia formed shortly after Charon did and has been stable, albeit gradually losing volume, over the age of the Solar System.

The western lobe of the icy, heart-shaped feature on Pluto, provisionally called Sputnik Planitia (Extended Data Fig. 1), is composed of a mixture of nitrogen, methane and carbon monoxide ices[1,6,7]—substances that are volatile at the temperatures expected on Pluto (about 40 K). Its location at 30° N—a latitude that is temperate on Earth—currently receives substantially less solar energy per Pluto year than all other latitudes. Furthermore, the axial tilt and orbital eccentricity of Pluto evolve on million-year timescales[8,9], leading to important changes in the annual energy flux to the dwarf planet and to climate variations that are analogous to ice-age cycles on Earth. We investigate these variations[10–19] by considering the instantaneous flux of sunlight that is absorbed by a unit surface element on Pluto:

$$F = \frac{L}{4\pi r^2}(1 - A)\cos(\gamma) \quad (1)$$

where L is the solar luminosity, r is the Pluto–Sun distance, A is Pluto's albedo and γ is the angle between the Sun–Pluto line and the normal to the surface element.

We average equation (1) over one orbit of Pluto about the Sun (see Methods and Extended Data Fig. 2), assuming a perfect absorber ($A = 0$) to obtain the solar energy flux to different latitudes on Pluto. Pluto's current axial tilt (or obliquity) is $\epsilon = 120°$, but it varies from 104° to 127° over the course of a 2.8-million-year cycle[9]. Accordingly, we repeat the calculation for several different obliquities (Fig. 1). The curve for the present-day tilt has a minimum flux at 26.5° latitude, with more solar energy incident at the equator and substantially more at the poles. In the current epoch, Pluto's poles receive about 10% more solar energy than does its equator, but this ratio varies from about 45% more at $\epsilon = 104°$ to near parity at $\epsilon = 127°$. Volatiles are driven away from the poles during the long hot summers, preferentially migrating to regions with cooler climates[12]. Once deposited, these volatiles are more difficult to dislodge, resulting in thinner layers returning to the poles in winter. Over many repeated seasonal cycles, these processes inexorably move volatiles away from the poles and towards cooler regions. Current conditions near the equator, and especially near 30°, strongly favour the deposition and retention of volatiles.

Over the 2.8-million-year cycle of Pluto's obliquity, the equator is alternately more and less hospitable to the build up of ices than is 30° latitude. The flow of ices across the equator, as evidenced in Extended Data Fig. 1, might be due to the recent warming trend at the equator, which could be mobilizing the ices in the southernmost regions of Sputnik Planitia. Most importantly, conditions near 30° are remarkably constant over Pluto's full obliquity cycle, providing a stable climate in which to cultivate icy deposits over millions and even billions of years. Weaker effects of Pluto's orbital eccentricity and radiation from Charon are considered in Methods.

If incident sunlight was the only factor in determining the location of frozen volatiles on Pluto, then planet-encircling bands of ices centred near ±30° would be expected. However, the surface albedo of the planet determines the fraction of incident energy that is actually absorbed by Pluto. Dark areas in Extended Data Fig. 1 absorb about 85% of the incident sunlight ($A = 0.15$ in equation (1)), whereas the bright ices of Sputnik Planitia reflect a comparable fraction of incident sunlight back into space ($A \approx 0.85$)[6]. Owing to diminished absorption of sunlight, temperatures over bright icy regions should be much lower than over darker regions, thereby enhancing the deposition rate of volatiles and inhibiting sublimation[17]. The strong effect of albedo can drive longitudinal variations in ice cover. The dark equatorial regions of Pluto remain dark by discouraging deposition of bright frost layers, whereas the bright areas attract additional frost. The equally marked albedo variations on Saturn's moon Iapetus are driven by similar processes[20]. Acting in concert with variations in incident sunlight, albedo differences will cause volatiles to be preferentially deposited on the brightest terrain in the ±30° latitude bands. Perhaps the most likely trigger for the formation of Sputnik Planitia was bright terrain formed from refreezing of melt produced by a mid-sized impactor or an early period of cryovolcanism. Shadowing by mountains or in craters are also possibilities, although these are probably weaker effects. In any case, once ices begin to be deposited in one area, they raise the albedo and reflect more sunlight back to space. Thus, the absorption of energy decreases, sublimation is inhibited and deposition of more ices is enhanced, leading to a runaway process (Fig. 2; see Methods for more details). Runaway ice-cap formation on Pluto is the reverse of the accelerating melting that is now ongoing in Earth's north polar ice pack.

[1]University of Maryland, College Park, Maryland, USA. [2]SWRI, Boulder, Colorado, USA. [3]NASA Ames, Mountain View, California, USA.
*A list of participants and their affiliations appears at the end of the paper.

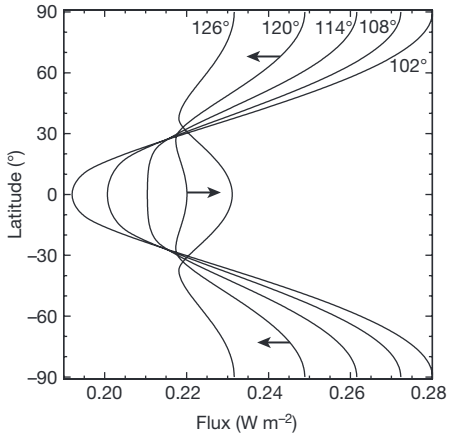

Figure 1 | Effects of Pluto's obliquity on insolation. We plot the orbit-averaged incident solar energy flux, or insolation, as a function of latitude on Pluto for five different values of Pluto's axial tilt ϵ. All curves were computed assuming the present-day value of Pluto's eccentricity, $e = 0.25$. The change in Pluto's tilt is the largest single factor that affects the strength of incident sunlight; the 1.4-million-year swing from $\epsilon = 104°$ to $\epsilon = 127°$ causes a change of roughly 20% in the flux absorbed at Pluto's equator and poles. Latitudes near $\pm 30°$ have a far more muted response to changes in Pluto's obliquity. The black arrows highlight the present-day obliquity of Pluto and show how the obliquity will change in the future; the minimum insolation at the equator occurred about 0.85 million years ago and the peak is due in about 0.55 million years.

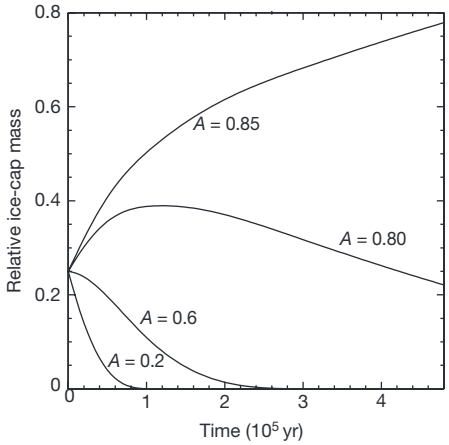

Figure 2 | The runaway albedo effect. This simulation tracks the time evolution of four ice caps with initially equal mass, each with an initial radius of 800 km and an average depth of 500 m, but with different albedos A. In reality, one feature probably dominated immediately after ices first started condensing out of the atmosphere, leading to much faster formation than is depicted here. Nevertheless, in each seasonal cycle of 248 years, we assume that a fraction $f = 0.5$ of absorbed solar energy converts ice to vapour, which is then redeposited on the ice caps in proportion to their exposed surface areas. As ice caps gain or lose mass, their areal coverage and average depth evolve as well, such that the ratio of diameter to depth remains constant. The darker two ice caps ($A = 0.2$ and $A = 0.6$) efficiently absorb solar energy and sublimate away rapidly, while the brighter two ($A = 0.8$ and $A = 0.85$) initially grow. Eventually, the brighter two ice caps compete more directly for the available vapour, and the one with the higher albedo captures all of the available ice, growing to a depth of 700 m and a radius of 1,270 km. Finally, the depth-to-diameter ratio of the surviving ice cap will grow as the lower-albedo margins preferentially sublimate in a process analogous to that considered here.

Owing to the strength of even a thin lithosphere, the initial ice deposits would have had positive topography contributing to a global longitudinal asymmetry. Such asymmetry would be subject to tidal torques from Charon that would act to rotate the ice cap towards the Pluto–Charon line. This probably occurred very early, within a few million years after Pluto and Charon were formed by the impact of two large Kuiper belt objects[21]. Prior to this giant impact, the surfaces of each of the objects were probably cold and covered with frozen volatiles and thin atmospheres. The collision produced either a mostly intact Charon or a circum-Pluto disk out of which Charon subsequently accreted; it also substantially heated portions of each body[21]. Tides acting between Pluto and Charon then despun each object and separated them on a timescale of the order of a few million years[9,22–24].

Far shorter timescales are sufficient for surface temperatures of Pluto to come back into equilibrium with the flux of solar energy and, accordingly, for most of Pluto's volatiles to freeze out onto its surface. Deposition would occur preferentially at latitudes near the equator if Pluto's obliquity then was below 114°, or nearer latitudes of $\pm 30°$ for larger obliquities (Fig. 1), and at longitudes with favourably high albedos. Over many seasonal cycles of sublimation and deposition, the runaway albedo effect (discussed above and in Methods) will cause a single ice cap to form in at most a few hundred thousand years. As Charon approached its current distance from Pluto, the obliquity of the dwarf planet stabilized to something like its current value, and Charon locked into synchronous orbit above a particular spot on Pluto's surface. The ice cap was plausibly the largest contributor to global topography (see Methods), dwarfing in horizontal scale the mountains and craters scattered across Pluto's surface. In this circumstance, Charon would cease moving relative to Pluto's surface when it reached one of two equilibrium longitudes: that of the ice cap itself or 180° further on (see Fig. 3 and Methods). For this type of tidal alignment, all that is needed is for the ice cap to control the longitudinal asymmetry of Pluto when averaged over broad 90° swaths of longitude. On these large scales, the gravitational signature from the mass of the ice cap exceeds the integrated effect of Pluto's other topography. The vertical and horizontal extent of the ice cap is also relatively unimportant, and it is sufficient for the ice to initially simply fill in topographical lows. The runaway albedo effect, acting over time, probably concentrated the ice into the deep convecting structure that we now observe (see Methods). The current position of Sputnik Planitia, centred nearly opposite the sub-Charon longitude of 0°, provides excellent support for this idea of moon-driven tidal alignment. Indeed, if randomly placed, there is only an approximately 10% chance that the ice cap would fall within 10° of one of the two critical longitudes, 0° and 180°.

Once Charon comes to rest above Pluto, the gravity of the satellite sets up a permanent tidal bulge on the dwarf planet that reinforces the position of the ice cap at a longitude that intersects the Pluto–Charon line. This permanent bulge holds the ice cap in place even against substantial mass loss of volatiles from the ice cap to the atmosphere, space or elsewhere on the planet. The ice cap would rotate away from 180° longitude only if enough ice was moved to reveal a large negative gravity anomaly, or basin, and the basin would have to be sufficiently large and deep to overcome the permanent tidal bulge. Therefore, once locked in, the ice cap will remain near its current equilibrium longitude of 180° against all but the most extreme changes. Moderately sized ice caps would also move slightly towards the equator[2,4,25], but such motions are resisted by Pluto's rotational bulge. Furthermore, any equatorward displacement of the ice cap, or indeed even an initially equatorial ice cap, would be affected by many thousands of annual sublimation and deposition cycles that would move the ice cap slowly poleward towards the latitudes with the least orbit-averaged flux of sunlight (see Methods). The north–south orientation of Sputnik Planitia may provide some evidence for such motions. Eventually conditions stabilized, leaving Pluto with a single dominant ice cap centred on a latitude of 25° determined by a minimum of solar illumination and a longitude of 175° set by long-ago tidal forces from Charon. Therefore, Pluto should be in one of four possible end states: with an ice cap centred near 30° or −30° latitude and near 0° or 180° longitude. Positions within 10° of these end states cover just 3% of Pluto's surface, making Sputnik Planitia's location near one of them particularly noteworthy.

The ices within Sputnik Planitia contain solid-state convection cells that suggest depths of several kilometres[1,26,27]. Convection works to

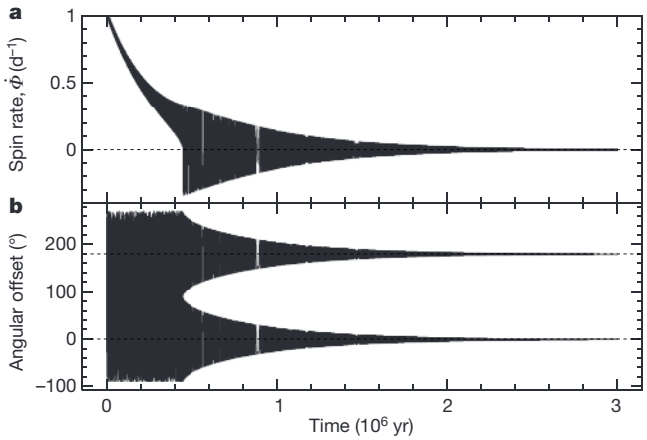

Figure 3 | Tidal locking of Pluto. a, The spin rate of Pluto relative to Charon's orbital motion ($\dot{\Phi}$) is shown for two separate initial conditions differing in phase by 180°. The two curves are plotted on top of one another (see Methods). Torques from Charon on the tidal bulges that are raised on Pluto by the moon act to slow Pluto's relative spin rate towards zero, where it ultimately locks to Charon's orbital rate ($\dot{\Phi} = 0$, indicated by the dashed line) to form the doubly synchronous system that we observe today. **b**, The longitudinal offset between Charon and the ice cap on Pluto's surface is shown for the two initial conditions. After a time of rapid rotation, each simulated Pluto is captured into libration about an equilibrium point, one with the longitudes of Pluto's ice cap and Charon aligned and the other with them separated by 180°; these critical longitudes are marked by dashed lines.

keep the surface bright by continually exposing fresh ice and reprocessing dirty ice, protecting the ice cap against additional absorption of sunlight. Despite its thickness, the surface of Sputnik Planitia is actually a topographic low relative to the global average, residing in a large basin[26]. This depression has been interpreted as having an impact origin[2,26,28]—a scenario that is not wholly inconsistent with our arguments; such a structure might, for example, be created by the loss shortly after its formation of a hypothetical moon similar to the four that currently reside outside Charon's orbit[1,29]. However, there is a simpler alternative: mass loading of Pluto's surface with a layer of ice many kilometres thick early in Pluto's history when its rigid lithosphere was thin would depress the surface substantially; the ice cap would make its own basin. This interpretation has the advantage of providing an explanation for why the basin is coincident with the ice cap and why both are located at the coldest latitude on Pluto and at a longitude that is directly opposite Charon. Because nitrogen ice and the water-ice bedrock have comparable densities, the nitrogen ice cap would have efficiently depressed the pre-existing landscape. In this case, the fact that the volume of the basin substantially exceeds that of Sputnik Planitia itself[26] implies that some of the ices that once filled the basin are now elsewhere, possibly lost to space over billions of years[30,31], hidden in the unlit southern hemisphere or buried underneath equatorial or other deposits. In addition, bulk movement of the ices on million-year precessional timescales may have eroded the regions around Sputnik Planitia, further enlarging the basin.

Online Content Methods, along with any additional Extended Data display items and Source Data, are available in the online version of the paper; references unique to these sections appear only in the online paper.

Received 30 May; accepted 28 October 2016.

1. Stern, S. A. *et al.* The Pluto system: initial results from its exploration by New Horizons. *Science* **350,** aad1815 (2015).
2. Nimmo, F. *et al.* Reorientation of Sputnik Planitia implies a subsurface ocean on Pluto. *Nature* http://dx.doi.org/10.1038/nature20148 (2016).
3. Bertrand, T. & Forget, F. Observed glacier and volatile distribution on Pluto from atmosphere–topography processes. *Nature* http://dx.doi.org/10.1038/nature19337 (2016).
4. Keane, J. T., Matsuyama, I., Kamata, S. & Steckloff, J. K. Reorientation and faulting of Pluto due to volatile loading within Sputnik Planita. *Nature* http://dx.doi.org/10.1038/nature20120 (2016).
5. Spada, G. *et al.* Greenland uplift and regional sea level changes from ICESat observations and GIA modelling. *Geophys. J. Int.* **189,** 1457–1474 (2012).
6. Grundy, W. M. *et al.* Surface compositions across Pluto and Charon. *Science* **351,** aad9189 (2016).
7. Protopapa, S. *et al.* First look at global Pluto's surface composition through pixel-by-pixel radiative scattering model of New Horizons Ralph/LEISA data. *Icarus* (in the press); preprint at https://arxiv.org/abs/1604.08468 (2016).
8. Dobrovolskis, A. R. & Harris, A. W. The obliquity of Pluto. *Icarus* **55,** 231–235 (1983).
9. Dobrovolskis, A. R., Peale, S. J. & Harris, A. W. in *Pluto and Charon* (eds Stern, S. A. & Tholen, D. J.) 159–190 (Univ. Arizona Press, 1997).
10. van Hemelrijck, E. The insolation at Pluto. *Icarus* **52,** 560–564 (1982).
11. van Hemelrijck, E. Insolation changes on Pluto caused by orbital element variations. *Earth Moon Planets* **33,** 163–177 (1985).
12. Binzel, R. P. 1991 Urey prize lecture: physical evolution in the solar system—present observations as a key to the past. *Icarus* **100,** 274–287 (1992).
13. Spencer, J. R. *et al.* in *Pluto and Charon* (eds Stern, S. A. & Tholen, D. J.) 435–473 (Univ. Arizona Press, 1997).
14. Lissauer, J. J., Barnes, J. W. & Chambers, J. E. Obliquity variations of a moonless Earth. *Icarus* **217,** 77–87 (2012).
15. Earle, A. M. & Binzel, R. P. Pluto's insolation history: latitudinal variations and effects on atmospheric pressure. *Icarus* **250,** 405–412 (2015).
16. Hamilton, D. P. The icy cold heart of Pluto. In *47th Division for Planetary Sciences Meeting* abstr. **200.07** (American Astronomical Society, 2015).
17. Earle, A. M. *et al.* Long-term surface temperature modeling of Pluto. *Icarus* http://dx.doi.org/10.1016/j.icarus.2016.09.036 (2016).
18. Binzel, R. P. *et al.* Climate zones on Pluto and Charon. *Icarus* http://dx.doi.org/10.1016/j.icarus.2016.07.023 (2016).
19. Nadeau, A. & McGhee, R. A. A simple method for calculating a planet's mean annual insolation by latitude. Preprint at https://arxiv.org/abs/1510.04542 (2015).
20. Spencer, J. R. & Denk, T. Formation of Iapetus' extreme albedo dichotomy by exogenically triggered thermal ice migration. *Science* **327,** 432–435 (2010).
21. Canup, R. M. A giant impact origin of Pluto-Charon. *Science* **307,** 546–550 (2005).
22. Peale, S. J. in *Planetary Satellites* (ed. Burns, J. A.) 87–111 (Univ. Arizona Press, 1977).
23. Murray, C. D. & Dermott, S. F. *Solar System Dynamics* **165** (Cambridge University Press, 2000).
24. Cheng, W. H., Lee, M. H. & Peale, S. J. Complete tidal evolution of Pluto–Charon. *Icarus* **233,** 242–258 (2014).
25. Matsuyama, I., Mitrovica, J. X., Manga, M., Perron, J. T. & Richards, M. A. Rotational stability of dynamic planets with elastic lithospheres. *J. Geophys. Res. Planets* **111,** E02003 (2006).
26. Moore, J. M. *et al.* The geology of Pluto and Charon through the eyes of New Horizons. *Science* **351,** 1284–1293 (2016).
27. McKinnon, W. B. *et al.* Convection in a volatile nitrogen-ice-rich layer drives Pluto's geological vigour. *Nature* **534,** 82–85 (2016).
28. Johnson, B. C., Bowling, T. J., Trowbridge, A. J. & Freed, A. M. Formation of the Sputnik Planum basin and the thickness of Pluto's subsurface ocean. *Geophys. Res. Lett.* **43,** 10068–10077 (2016).
29. Showalter, M. R. & Hamilton, D. P. Resonant interactions and chaotic rotation of Pluto's small moons. *Nature* **522,** 45–49 (2015).
30. Gladstone, G. R. *et al.* The atmosphere of Pluto as observed by New Horizons. *Science* **351,** aad8866 (2016).
31. Bagenal, F. *et al.* Pluto's interaction with its space environment: solar wind, energetic particles, and dust. *Science* **351,** aad9045 (2016).

Acknowledgements We thank NASA for its support of the New Horizons mission and the New Horizons mission team for making the July 2015 flyby possible. We thank V. Bray, B. Carcich, J. Hofgartner and F. Nimmo for helpful comments. This research was supported by a grant from NASA Origins (to D.P.H.).

Author Contributions D.P.H. wrote the manuscript and the computer codes used to produce all of the figures. S.A.S., L.A.Y. and J.M.M. commented on draft manuscripts and have leadership roles with New Horizons that helped make the mission possible.

Author Information Reprints and permissions information is available at www.nature.com/reprints. The authors declare no competing financial interests. Readers are welcome to comment on the online version of the paper. Correspondence and requests for materials should be addressed to D.P.H. (dphamil@umd.edu).

New Horizons Geology, Geophysics & Imaging Theme Team

R. P. Binzel[1], M. W. Buie[2], B. J. Buratti[3], A. F. Cheng[4], K. Ennico[5], W. M. Grundy[6], I. R. Linscott[7], W. B. McKinnon[8], C. B. Olkin[2], H. J. Reitsema[9], D. C. Reuter[10], P. Schenk[11], M. R. Showalter[12], J. R. Spencer[2], G. L. Tyler[7] & H. A. Weaver[4]

[1]MIT, Cambridge, Massachusetts, USA. [2]SWRI, Boulder, Colorado, USA. [3]JPL, Pasadena, California, USA. [4]Applied Physics Lab, Laurel, Maryland, USA. [5]NASA Ames, Mountain View, California, USA. [6]Lowell Observatory, Flagstaff, Arizona, USA. [7]Stanford University, Stanford, California, USA. [8]Washington University, St Louis, Missouri, USA. [9]Ball Aerospace, Denver, Colorado, USA. [10]NASA Goddard, Greenbelt, Maryland, USA. [11]Lunar and Planetary Institute, Houston, Texas, USA. [12]SETI Institute, Mountain View, California, USA.

METHODS

Solar energy deposition on Pluto. We begin by averaging the energy flux from sunlight to a given latitude l_y on Pluto over the course of one Pluto rotation. The integration is over time with $P_{\rm day}$ equal to one Pluto day or approximately 6.39 Earth days. The daily average flux to a given latitude is given by the integral of equation (1) with $A=0$:

$$\overline{F}_{\rm day}=\frac{L}{4\pi r^2}\frac{1}{P_{\rm day}}\int_0^{P_{\rm day}}\cos(\gamma)\mathrm{d}t=\frac{L}{4\pi r^2}\frac{1}{\pi}\int_0^{\beta_{\max}}\cos(\gamma)\mathrm{d}\beta \tag{2}$$

where L is the solar luminosity and r is the instantaneous Pluto–Sun distance, which is assumed to remain approximately constant over one Pluto day. The angle γ is the angular distance between the Sun and the point of interest on Pluto's surface (Extended Data Fig. 2); γ changes continuously in time owing to Pluto's rotation. We have used the fact that β—the hour angle measured from the north pole (Extended Data Fig. 2)—increases uniformly as Pluto rotates so that $\beta/(2\pi)=t/P_{\rm day}$. Finally, $\beta_{\max}$ is the largest β such that the Sun is still visible ($\gamma=90°$). Equation (2) shows that the daily average flux is highest when both $\beta_{\max}$ and $\cos(\gamma)$ are maximized (long sunlit periods with the Sun nearly overhead); this situation is approximately realized at two locations along the orbit of Uranus where that planet's spin axis points nearly at the Sun.

The integral is evaluated by expanding the angle γ with the law of cosines for the spherical triangle shown in Extended Data Fig. 2. We obtain the following result[32,33]:

$$\overline{F}_{\rm day}=\frac{L}{4\pi r^2}\frac{1}{\pi}[\beta_{\max}\sin(l_s)\sin(l_y)+\sin(\beta_{\max})\cos(l_s)\cos(l_y)] \tag{3}$$

where l_s is the subsolar latitude, l_y is the latitude of interest and $\cos(\beta_{\max})=-\tan(l_s)\tan(l_y)$, with $\beta_{\max}\in[0,\pi]$. For circular orbits about the Sun, note the symmetries $\overline{F}_{\rm day}(l_s,l_y)=\overline{F}_{\rm day}(-l_s,-l_y)$ and $\overline{F}_{\rm day}(l_s,l_y)=\overline{F}_{\rm day}(l_y,l_s)$. Equation (3) can be used to show that, on the summer solstice, Pluto's summer pole receives nearly 5.5 times the energy than its equator does. In fact, Pluto receives more daily sunlight at its north pole than at its equator whenever $l_s>17.66°$. For higher latitudes, the more direct sunlight to the equator is more than offset by the greater amount of time that the polar regions spend in sunlight. Of course, the equator is sunlit for exactly half a Pluto rotation at all times of the year. For a given position of the Sun north of the equator, the greatest daily flux of energy is always to a more northernly latitude. For example, the daily flux to latitude $l_y=17.66°$ when $l_s=17.66°$ is less than that to all latitudes l_y between 17.66° and 41.8°.

To determine the annually averaged energy flux, we integrate equation (3) over a full Pluto year:

$$\overline{F}_{\rm year}=\frac{L}{4\pi}\frac{1}{\pi}\frac{1}{P_{\rm year}}\int_0^{P_{\rm year}}\frac{1}{r^2}[\beta_{\max}\sin(l_s)\sin(l_y)+\sin(\beta_{\max})\cos(l_s)\cos(l_y)]\mathrm{d}t$$

We use Kepler's second law

$$\frac{\mathrm{d}\nu}{\mathrm{d}t}=\frac{h}{r^2} \tag{4}$$

to replace integration over time with an integration over the angle ν. Here $h=\sqrt{GM_\odot a(1-e^2)}$ is Pluto's constant orbital angular momentum per unit mass, a, e and ν are Pluto's orbital semimajor axis, eccentricity and true anomaly, respectively, G is the gravitational constant and $M_\odot$ is the solar mass. The true anomaly is the angle between Pluto and its orbital pericentre as measured from the Sun. Note that the r^2 introduced by this change of variables conveniently cancels the r^{-2} from the definition of flux. We find

$$\overline{F}_{\rm year}=\frac{L}{8\pi^3}\frac{1}{a^2\sqrt{1-e^2}}\int_0^{2\pi}[\beta_{\max}\sin(l_s)\sin(l_y)+\sin(\beta_{\max})\cos(l_s)\cos(l_y)]\mathrm{d}\nu \tag{5}$$

Together, the true anomaly ν, its time derivative (equation (4)) and the argument of latitude u defined by

$$\sin(u)=\sin(\epsilon)\sin(l_s) \tag{6}$$

give full information about the apparent motion of the Sun as seen from Pluto. The argument of latitude is the angle between the present-day position of the Sun and its position when it crosses Pluto's equator heading north; ϵ is Pluto's obliquity. The true anomaly and argument of latitude are related by $u=w+\nu$, where w is the argument of pericentre; $w=0$ occurs at times when Pluto is closest to the Sun at its spring equinox. Because the integrand is a complicated function of the true anomaly, the integral in equation (5) must be evaluated numerically.

Although intractable, the integral displays some interesting symmetries. First, taking $\epsilon\to\pi-\epsilon$ leaves equation (6) unaltered and so $\overline{F}_{\rm year}(\epsilon,l_y)=\overline{F}_{\rm year}(\pi-\epsilon,l_y)$. Consequently, Pluto, with a tilt of $\epsilon=120°$, gets the same annual insolation pattern on its surface as a planet tilted by $\epsilon=60°$. More remarkably, if we rewrite the equation as an integral over u using $\mathrm{d}u=\mathrm{d}\nu$, the limits of integration cover a full cycle of the Sun around Pluto and can be returned to the range $[0,2\pi]$. Therefore, the integral does not depend in any way on the location of Pluto's pericentre[9]. The only effect of Pluto's highly eccentric orbit on $\overline{F}_{\rm year}$ comes from the overall scaling factor outside the integral[33]. This means that the annual average energy flux to any latitude on Pluto is most easily determined by treating its orbit as circular for the integration in equation (5), and then adjusting the scaling factor outside the integral (see Extended Data Fig. 3).

A final symmetry comes from flipping the subsolar point and the latitude of interest to the opposite hemisphere with the transformation $l_s\to-l_s$ and $l_y\to-l_y$. This flipping occurs when the Sun is half an orbit further along ($u\to u+\pi$), so $\mathrm{d}u\to\mathrm{d}u$ and we rewrite the integration limits as before. Therefore, $\overline{F}_{\rm year}(\epsilon,l_y)=\overline{F}_{\rm year}(\epsilon,-l_y)$ and the annual energy flux to a planet is always symmetric about its equator. This symmetry, which is clearly visible in Fig. 1, is seen in some works[10,11,14,17,19], but not others[13,15].

The solution of equation (5) shows that cold polar regions as exist on Earth or Mars require obliquities of less than 45° or more than 135°, whereas deep equatorial minima occur for all planets tilted between 66° and 114°. Pluto's obliquity varies around the 114° boundary, spending about 1.3 million years with an equatorial minimum followed by 1.5 million years with minima at low to mid latitudes (Fig. 1).

Numerical techniques. We wrote several codes in C to calculate the energy flux from the Sun for different orbital geometries and axial tilts over various time intervals. We evaluate equation (3) directly to quickly determine average daily fluxes at different times during Pluto's year; to obtain annual averages, we evaluate equation (5). For averages over one Pluto year, millions of years in the past or future, we update Pluto's orbital parameters and tilt appropriately[9] and again evaluate equation (5).

As seen from Pluto, Charon is an extremely large and extremely close satellite, appearing fully seven times larger than the full Moon in Earth's sky, which itself is larger than any other planetary satellite seen from its primary. Moreover, owing to its tidally evolved state, Charon hovers over one point on Pluto's equator, continuously illuminating the same hemisphere. Accordingly, we investigate the reflected sunlight and thermal infrared emission from Charon on ices on Pluto's surface. Because Charon holds its position over a single spot on Pluto's equator, the angle between this spot and the position of interest γ_C is constant. We estimate the average flux of solar energy that comes to Pluto via Charon as follows:

$$\overline{F}_{\rm C,year}=\overline{F}_{\rm year}\frac{1}{2}\frac{R_C^2}{a_C^2}\cos(\gamma_C) \tag{7}$$

where R_C is Charon's radius and a_C is its distance from Pluto. Here we have assumed that Charon is full as seen from Pluto, have treated Charon as a slow rotator and have made simplifying assumptions about how its surface reflects sunlight. We have made use of $\overline{F}_{\rm year}$ from equation (5), which introduces errors of approximately 20%. Charon's phases vary over a Pluto year, always oscillating about, but rarely departing appreciably from, half full; in the spirit of estimation, we ignore these subtleties, but recognize that our full-moon approximation is an overestimate. Additionally, we underestimate the effects of Charon's thermal emission because equation (7) determines the energy incident on Pluto rather than the energy absorbed. More than half of the sunlight incident on Charon is reprocessed into thermal infrared, which delivers energy to ices far more efficiently than does visible light. Finally, more indirect energy from Charon is delivered to the night side of Pluto than to the dayside, which probably has consequences that are not captured by our approach of considering only annual averages. We also estimate the effect of sunlight reductions to Pluto due to eclipses by Charon that occur every 124 years[34]. When averaged over a Pluto year, this effect is smaller, but not substantially smaller, than reflected sunlight and thermal emission from Charon. With all of these caveats, our estimate for contributions of Charon shine to Pluto's sub-Charon longitude is depicted in Extended Data Fig. 3; despite Charon's size and proximity, these effects are very small—roughly an order of magnitude weaker than the already weak effects of orbital eccentricity.

This analysis shows that variations in Pluto's obliquity and albedo are the strongest drivers of sublimation and deposition, with weaker but noticable effects from orbital eccentricity and even radiation from the large moon Charon. Although we find a slight preference for ices to be deposited on the anti-Charon hemisphere, the effect is too weak to account for the location of Sputnik Planitia.

Runaway albedo effect. To illustrate the runaway albedo effect, we developed a code to track the individual sizes of several spatially separated ice deposits through

Pluto's seasonal cycles. We assume that a fraction $1 - A$ of incident sunlight is absorbed by the ices, with A the albedo from equation (1). We further assume that a fraction f of absorbed sunlight converts ice to vapour during sunlight hours and that all of this vapour redeposits onto the ice caps at night. The rest of the incident energy goes to heating of the surface and subsurface layers, and redeposition is assumed to be in proportion to the exposed surface areas of the ice caps. Over a single summer day ice preferentially sublimates into the atmosphere, whereas in winter the converse is true. We consider only the longer annual cycle, assuming that the vapour content of the atmosphere remains constant and using it only as a conduit for communication from one ice deposit to another. We set the number of ice caps, and their sizes, depths and albedos as initial conditions, and track changes to the deposits over many annual cycles. Figure 2 shows a typical run with four large ice caps of initially equal size, but different albedos. The four-ice-cap situation in Fig. 2 is unlikely to have ever occurred on Pluto, but serves as an effective demonstration of the power of the runaway albedo effect.

Albedos are macroscopic averages, encoding the effects of large-scale surface topography as well as compositional differences. The ice caps may be placed at arbitrary locations on Pluto's surface, but here we consider caps near a configuration in which each spot receives the same annual solar insolation. The total mass in ice is set to approximate that believed to be in the ice cap today, and is preserved over the course of the simulation. We find that mass is rapidly removed from the darker two ice caps, owing to their more efficient absorption of solar radiation and consequent copious production of vapour. Simultaneously, the brighter two ice caps both grow in mass and spatial extent, with their larger surface areas attracting more of the available vapour each annual cycle. Ultimately, and on relatively short timescales, only one ice cap remains.

Although this simple model does not capture all of the relevant physics—for example, it does not include the expected brightening of the ice cap once its size exceeds that necessary for solid-state convection[27]—it effectively demonstrates that very small albedo differences are magnified to the point where only a single ice cap survives. Similar considerations explain why an excess of solar radiation at polar and equatorial latitudes drives ices towards latitudes that receive the least solar illumination (Fig. 1).

Tidal despinning of Pluto. We developed a numerical code to track how the angular orientation of Pluto relative to Charon changes as a result of tidal influences from the massive satellite. The relative spin rate of Pluto starts positive and then slows to zero, or tidally locks, over a timescale of about a million years[9,22–24], where it remains today. Gravitational torques from Charon on the tidal bulge raised on Pluto by this satellite cause a monotonic decrease in the spin rate of the dwarf planet. In addition, the dominant torques on the asymmetric shape of Pluto vary periodically at twice the relative spin rate. We show below that Pluto's asymmetric shape is probably dominated by its ice cap. These two effects are captured by the following equation for the rotational acceleration of Pluto:

$$\frac{\mathrm{d}^2\Phi}{\mathrm{d}t^2} = \epsilon_1 \mathrm{sign}\left(\frac{\mathrm{d}\Phi}{\mathrm{d}t}\right) + \epsilon_2 \sin(2\Phi) \qquad (8)$$

where Φ is the rotational phase of Pluto relative to Charon, t is time, $\mathrm{d}\Phi/\mathrm{d}t$ is the relative spin rate, ϵ_1 is the tidal dissipation rate and ϵ_2 is set by the intrinsic shape of Pluto. The first term on the right-hand side of equation (8) captures tidal despinning of Pluto that occurs as a result of tides raised on that body by Charon. Here we use the so-called constant-Q formulation of tides[23], which, although in common usage, has a very obvious flaw. The tidal term takes a discontinuous step when $\mathrm{d}\Phi/\mathrm{d}t = 0$, which is unphysical. When $\mathrm{d}\Phi/\mathrm{d}t = 0$, which corresponds to the spin rate of Pluto precisely matching the orbital rate of Charon, the tidal bulge raised on Pluto by Charon is directly under the satellite and there can be no net torque. An infinitesimally faster or slower spin rate should lead to an infinitesimal torque that drives the system back towards $\mathrm{d}\Phi/\mathrm{d}t = 0$, not the macroscopic torque implied by equation (8). This formulation of tides also leads to numerical issues, because no step size in time is sufficiently small to resolve a step function. Accordingly, we smooth the second term in equation (8) by making it proportional to $\mathrm{d}\Phi/\mathrm{d}t$ when $|\mathrm{d}\Phi/\mathrm{d}t|$ is less than a specific threshold. This choice is more physical, maintains continuity, is numerically more stable and has the added advantage of making equation (8) linear; in fact, for small Φ it is the equation of a classic damped harmonic oscillator. In the code, this change takes the form of a single conditional statement. Taking nominal parameters in equation (4.165) from ref. 23, we calculate $\epsilon_1 = 1.4 \times 10^{-18}\ \mathrm{s}^{-2}$ and choose our threshold spin rate to be $\mathrm{d}\Phi/\mathrm{d}t = 1.0\ \mathrm{rad\ d}^{-1}$.

The last term in equation (8) characterizes torques from Charon on the longitudinally asymmetric shape of Pluto. Because Charon's distance is large compared to Pluto's radius, the global-scale topography (specifically the C_{22} quadrupolar component of topography) of Pluto determines its response to Charon. A single ice cap of mass m_{ice}, placed at the equator of an otherwise spherical planet, yields $C_{22} = m_{\mathrm{ice}}/(4M_{\mathrm{P}})$, where M_{P} is Pluto's mass; the contribution from an ice cap at 30° latitude is only 25% smaller. No dipole terms are produced by the addition of an ice cap as long as the origin of the system remains at Pluto's centre of mass. Therefore, a single ice cap of mass m_{ice} acts identically to two ice caps each of mass $m_{\mathrm{ice}}/2$ located 180° apart in longitude—a situation that is easier to visualize. For the parameters of the ice cap considered in Fig. 2, we have $m_{\mathrm{ice}}/M_{\mathrm{P}} = 3 \times 10^{-4}$, $C_{22} = 8 \times 10^{-5}$ and

$$\epsilon_2 = \frac{15}{4}\frac{GM_{\mathrm{P}}}{a_{\mathrm{C}}^3}\frac{m_{\mathrm{ice}}}{M_{\mathrm{P}}}\frac{M_{\mathrm{C}}}{M_{\mathrm{P}}} = 1.5 \times 10^{-14}\mathrm{s}^{-2}$$

where M_{C} is Charon's mass. Pluto's natural topography, if similar to Earth's, would yield a considerably smaller $C_{22} = 2.8 \times 10^{-6}$, providing support for our contention that Pluto's ice cap probably dominated the global topography. Substantial relaxation of Pluto towards spherical symmetry can occur without altering this conclusion.

The transformation $\Phi \rightarrow \Phi + \pi$ leaves equation (8) unaltered, which means that any trajectory that Φ follows has a second solution that is everywhere displaced from the first by 180°. When we integrate equation (8) in time, we find two equilibrium states that occur with equal probability: the ice cap can end up at Charon's longitude ($\Phi = 0$) or displaced by 180° to where the actual system is found. Figure 3 follows the evolution of Pluto's spin rate relative to Charon's orbit and the angular offset of the long axis of Pluto from Charon as a function of time. Because $\epsilon_2 \gg \epsilon_1$, the harmonic oscillator is underdamped and the system oscillates around the equilibrium point, within an envelope that decays exponentially. Our numerical simulations support our analytic discussion: we find rapid decay of Pluto's spin to a final state with the ice cap locked either to Charon's longitude or to roughly the observed configuration, each with 50% probability.

Code availability. The numerical codes used to produce Fig. 1 and Extended Data Fig. 3 are not publicly available. The codes developed to illustrate the runaway albedo effect (Fig. 2) and despinning of Pluto (Fig. 3) are available from D.P.H. on request.

Data availability. Data files used in the construction of the figures are available from D.P.H. on request.

32. Cross, C. A. The heat balance of the Martian polar caps. *Icarus* **15,** 110–114 (1971).
33. Ward, W. R. Climatic variations on Mars: 1. Astronomical theory of insolation. *J. Geophys. Res.* **79,** 3375–3386 (1974).
34. Buie, M. W., Tholen, D. J. & Horne, K. Albedo maps of Pluto and Charon: initial mutual event results. *Icarus* **97,** 211–227 (1992).

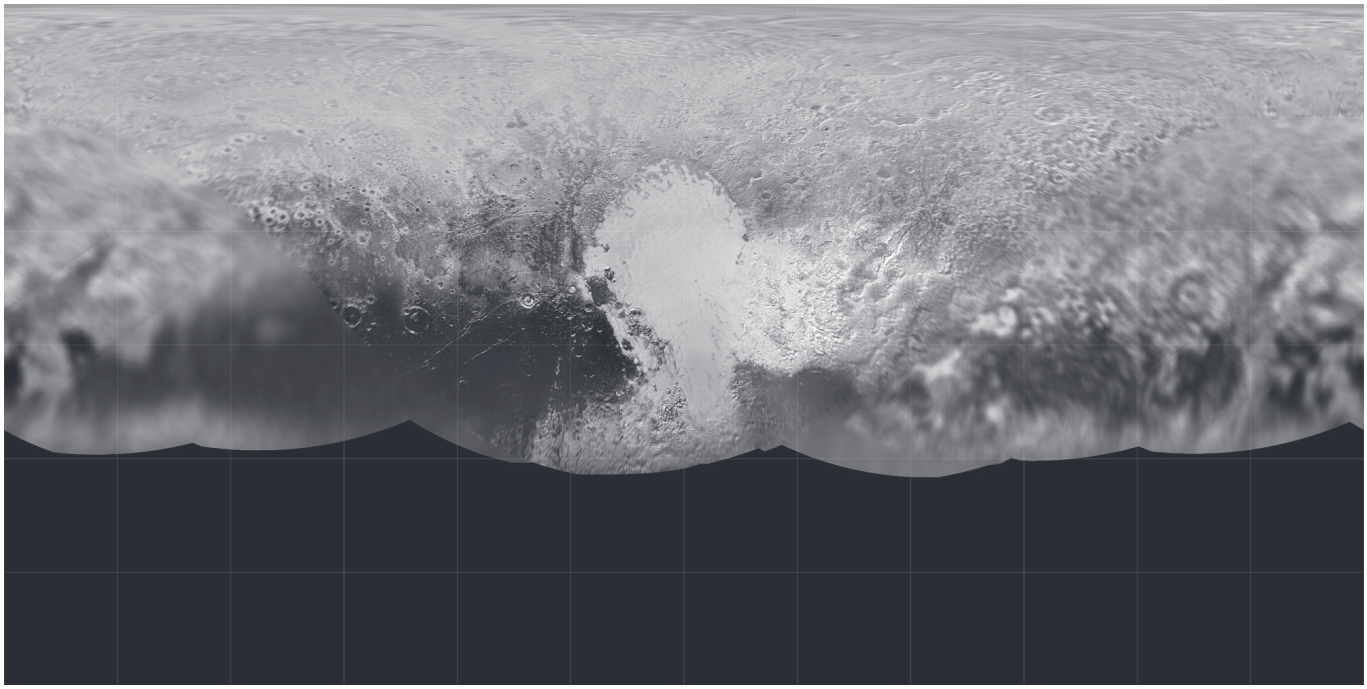

Extended Data Figure 1 | Surface map of Pluto. Sputnik Planitia, the informally named western lobe of the white heart-shaped feature, is approximately 1,000 km across and is centred on a latitude of 25° N and longitude of 175°, with the zero of longitude defined to run directly underneath Pluto's moon Charon. Owing to Pluto's slow rotation and the approach vector of New Horizons, the highest-resolution images were of Sputnik Planitia, and most other regions were imaged at much lower resolution from farther away. Consequently, this map is a mosaic of multiple images of differing resolution. Faint grid lines of latitude and longitude are spaced by 30°. Regions south of about 30° S were not sunlit and, hence, were not imaged, because they are currently experiencing polar night.

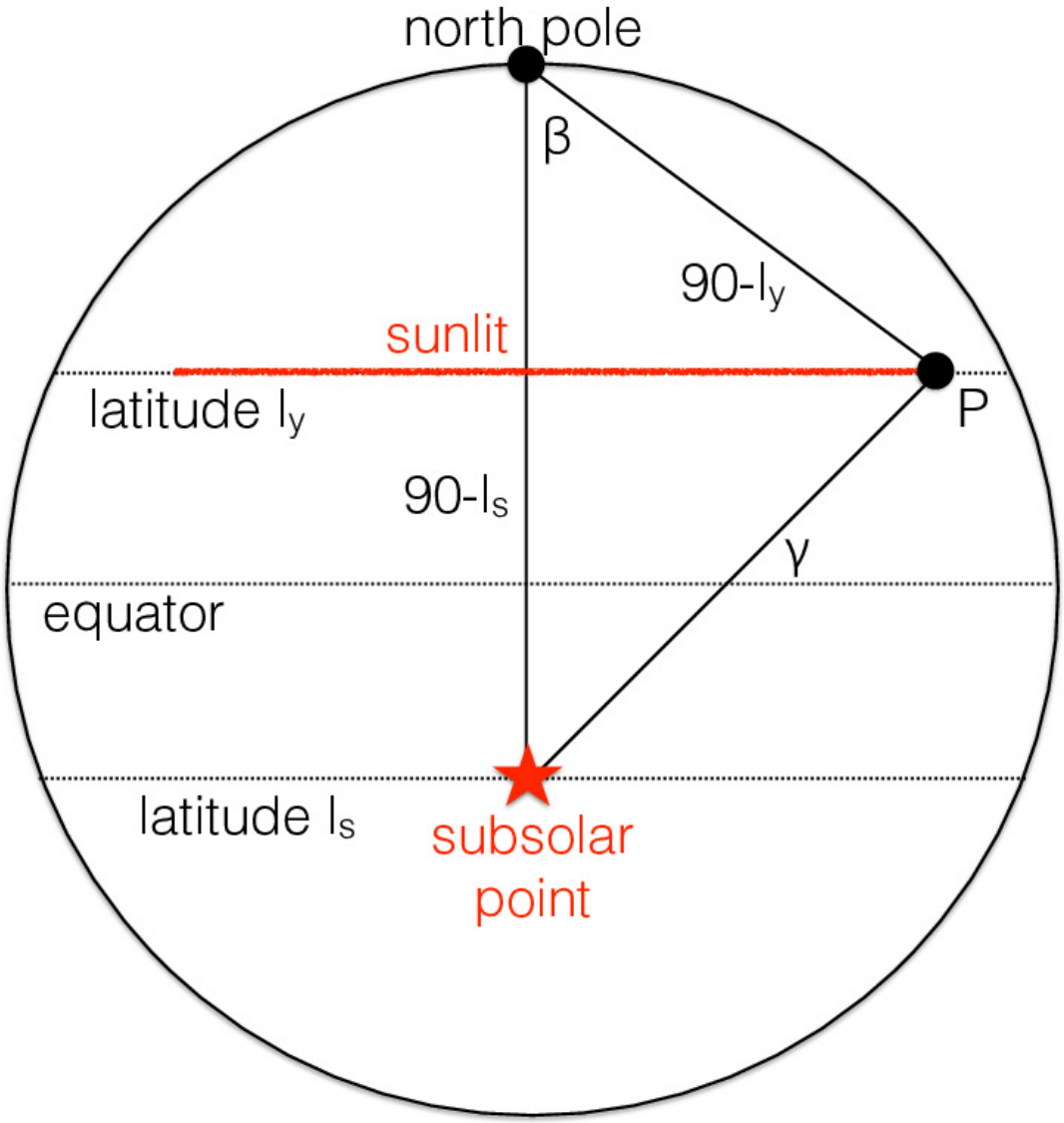

Extended Data Figure 2 | Geometry for energy deposition on Pluto. The large circle represents Pluto, with our view centred on the intersection of the equator and the noon meridian. At the location of the red star, the Sun is directly overhead, and it tracks along the latitude l_s over the course of a full rotation of Pluto. The thick horizontal red line segment shows the regions along latitude l_y that are currently illuminated by sunlight. The angle γ is the angular distance between the Sun and the point of interest on Pluto's surface (black dot labelled 'P' at latitude l_y), as measured from the centre of Pluto. The Sun is on the horizon when $\gamma = 90°$, which we define to occur at the meridional angle of $\beta = \beta_{max}$. The spherical triangle formed by γ and the two meridians connecting the north pole to the above-mentioned points defines γ in terms of the other variables and simplifies derivations of average energy fluxes.

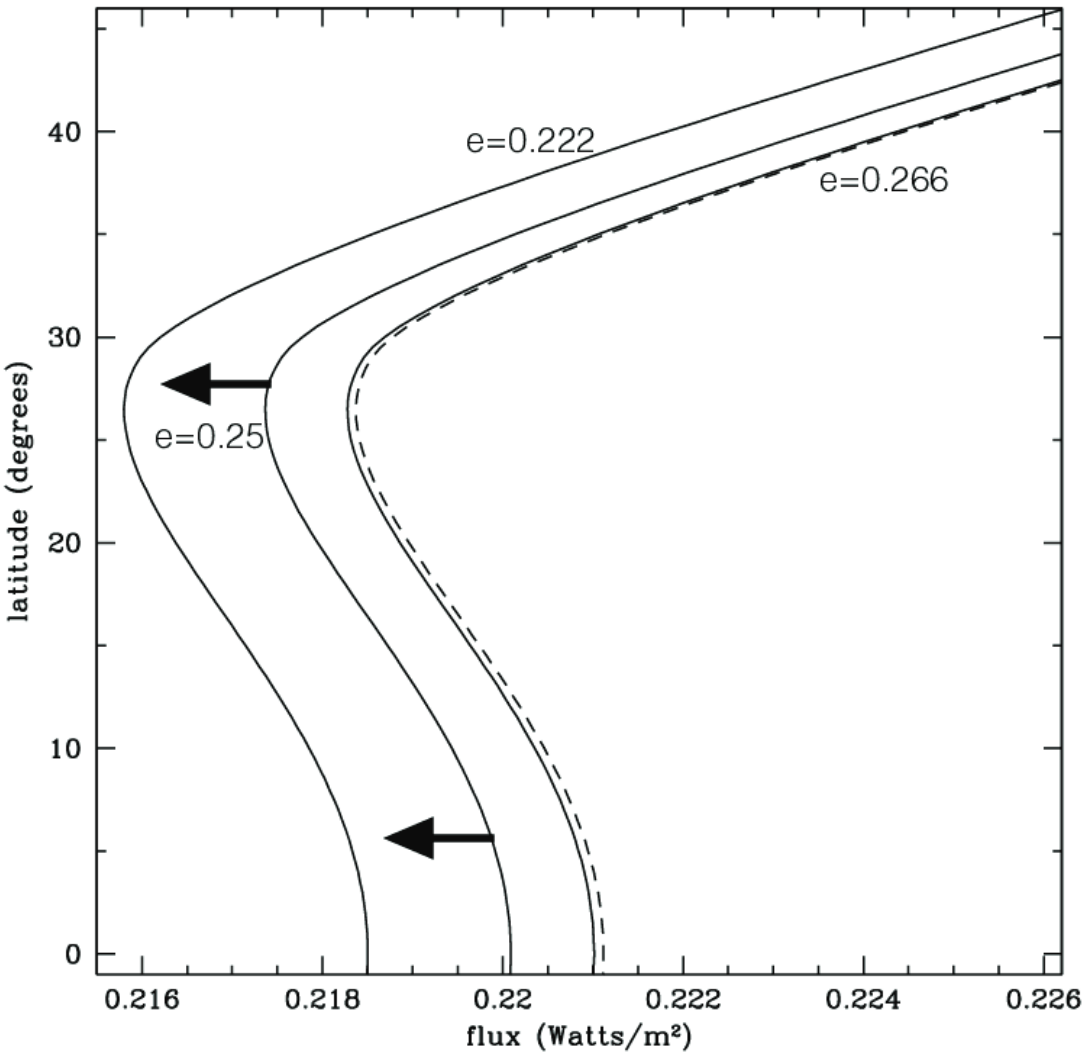

Extended Data Figure 3 | Effects of Pluto's eccentricity on insolation. Here we zoom in on the region surrounding Sputnik Planitia and show (solid curves) the solar energy flux with Pluto at its minimum ($e = 0.222$), current ($e = 0.25$) and maximum ($e = 0.266$) eccentricity, assuming a present-day obliquity of 120°. Black arrows show the future changes that are expected as a result of these eccentricity variations. As we show in Methods, Pluto's eccentricity affects insolation equally at all latitudes. Incident radiation from Charon, a 0.1% effect, moves the solid $e = 0.266$ curve slightly to the right, most noticeably at the equator, as indicated by the dashed curve and discussed in Methods. Eccentricity effects are at the 1% level, 20 times weaker than the obliquity effects highlighted in Fig. 1. The effect of Pluto's eccentricity varies with a 3.95-million-year period[8]. The maximum insolation to the entire planet occurred about 0.8 million years ago and the minimum will next occur in about 1.2 million years.